Investigation of Ion Binding in Chlorite Dismutases by Means of Molecular Dynamics Simulations

Axel Sündermann,[†] Maria M. Reif,[†] Stefan Hofbauer,[‡] Christian Obinger,[‡] and Chris Oostenbrink*,[†]

[†]Department of Material Sciences and Process Engineering, Institute of Molecular Modeling and Simulation, University of Natural Resources and Life Sciences Vienna, Muthgasse 18, A-1190 Vienna, Austria

[‡]Department of Chemistry, Division of Biochemistry, Vienna Institute of BioTechnology, University of Natural Resources and Life Sciences Vienna, Muthgasse 18, A-1190 Vienna, Austria

S *Supporting Information*

ABSTRACT: Chlorite dismutases are prokaryotic heme *b* oxidoreductases that convert chlorite to chloride and dioxygen. It has been postulated that during turnover hypochlorite is formed transiently, which might be responsible for the observed irreversible inactivation of these iron proteins. The only charged distal residue in the heme cavity is a conserved and mobile arginine, but its role in catalysis and inactivation is not fully understood. In the present study, the pentameric chlorite dismutase (Cld) from the bacterium *Candidatus Nitrospira defluvii* was probed for binding of the low spin ligand cyanide,

the substrate chlorite, and the intermediate hypochlorite. Simulations were performed with the enzyme in the ferrous, ferric, and compound I state. Additionally, the variant R173A was studied. We report the parametrization for the GROMOS force field of the anions ClO^-, ClO_2^-, ClO_3^-, and ClO_4^- and describe spontaneous binding, unbinding, and rebinding events of chlorite and hypochlorite, as well as the dynamics of the conformations of Arg173 during simulations. The findings suggest that (i) chlorite binding to ferric NdCld occurs spontaneously and (ii) that Arg173 is important for recognition and to impair hypochlorite leakage from the reaction sphere. The simulation data is discussed in comparison with experimental data on catalysis and inhibition of chlorite dismutase.
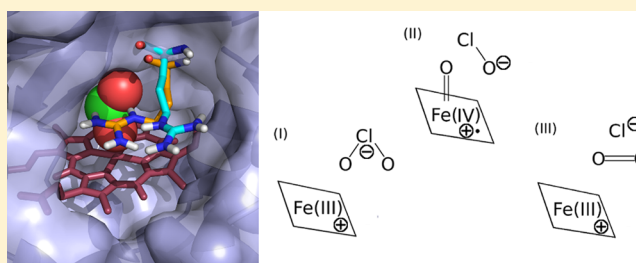
$\overset{\text{C}}{}$hlorite dismutases (Clds) are prokaryotic heme *b* oxido-reductases (EC 1.13.11.49) that convert chlorite to dioxygen and chloride. Based on subunit architecture and oligo-merization, two main clades are distinguished.[1−5] Clade 1 contains pentameric proteins including Cld from the bacterium *Candidatus Nitrospira defluvii* (NdCld), which was investigated in this work. In clade 2, dimeric representatives with smaller subunit size are found. Chlorite dismutases are suggested to have ancient roots since similar proteins were found in many different bacterial and archaeal phyla.[5,6]

Several crystal structures of Clds have been published in recent years;[3−5,7] these demonstrated that the only charged residue in the distal heme cavity is a conserved arginine residue, which was shown to be catalytically important but not essential for the degradation of chlorite.[5,8,9]

In the resting state, the heme iron of Cld is in the ferric state, which is stabilized by the imidazolate character of the proximal histidine.[7,10] It was shown by Hofbauer et al.[10] that the structural changes upon reduction of Cld to the ferrous form are very small, which is in agreement with other heme enzymes.[11−15] In NdCld, the chlorite access channel has a length of 1.5 nm with a bottleneck radius of 0.28 nm.[10] Chlorite (ClO_2^-) enters the channel and binds to ferric heme forming the Fe(III)−ClO_2 adduct. This induces the redox reaction, which includes the heterolytic cleavage of chlorite to hypochlorite (ClO^-) with

concomitant oxidation of ferric NdCld to the compound I state (which most probably is an oxoiron(IV) porphyrin radical). In the final reaction, hypochlorite recombines with the ferryl oxygen of compound I thereby releasing O_2 and chloride.[16]

In this postulated mechanism, several issues still need clarification including the question about the catalytic role of the distal arginine (i.e., Arg173 in NdCld). Crystal structures have shown that this basic amino acid can adopt two distinct conformations, either pointing toward the heme iron ("in") or toward the substrate channel entry ("out").[9] Mutational analyses suggested that the distal arginine is important to keep the transiently produced hypochlorite close to the ferryl oxygen for the rebound mechanism.[9,17] On the other hand, chlorite degradation can also occur in its absence, although significantly slower and with increased susceptibility for irreversible inactivation.[3−5,7,16,18−22] Hofbauer et al.[17] demonstrated that inactivation includes heme bleaching as well as oxidation and chlorination of amino acids of the protein moiety. The authors concluded that hypochlorite released from the active site during turnover is responsible for these modifications.[17]

Table 1. Detailed Overview of All Conducted Simulations with the Pentameric Chlorite Dismutase from *Candidatus Nitrospira defluvii*[a]

simulation	substrate	Arg173 starting position	heme state	ions	H$_2$O	initial box dimensions (L$_x$ × L$_y$ × L$_z$) [nm × nm × nm]	length [ns]
OC	ClO$_2^-$	out	ferric	50 Na$^+$, 20 Cl$^-$	29607	9.69 × 10.44 × 10.80	20
ON	CN$^-$	out	ferric	50 Na$^+$, 25 Cl$^-$	29590	9.69 × 10.44 × 10.80	20
OX	none	out	ferric	50 Na$^+$, 25 Cl$^-$	27510	9.30 × 10.35 × 10.69	20
RC	ClO$_2^-$	out	ferrous	50 Na$^+$, 15 Cl$^-$	29597	9.69 × 10.44 × 10.80	20
RN	CN$^-$	out	ferrous	50 Na$^+$, 20 Cl$^-$	29595	9.69 × 10.44 × 10.80	20
RX	none	out	ferrous	50 Na$^+$, 20 Cl$^-$	27390	9.30 × 10.33 × 10.7	20
CC	ClO$^-$	out	compound I	50 Na$^+$, 20 Cl$^-$	29640	9.69 × 10.44 × 10.81	20
CI	ClO$^-$	in	compound I	50 Na$^+$, 20 Cl$^-$	29598	9.69 × 10.44 × 10.81	20
MO	ClO$_2^-$	mutated to Ala	ferric	50 Na$^+$, 15 Cl$^-$	29215	9.50 × 10.51 × 10.82	20
MC	ClO$^-$	mutated to Ala	compound I	50 Na$^+$, 15 Cl$^-$	29207	9.50 × 10.50 × 10.82	20
OF	20 ClO$_2^-$ free in solution	out	ferric	50 Na$^+$, 20 Cl$^-$	29607	9.69 × 10.44 × 10.81	20
RF	20 ClO$_2^-$ free in solution	out	ferrous	50 Na$^+$, 20 Cl$^-$	29607	9.69 × 10.44 × 10.81	20

[a]The first column shows the label of the simulation; the second shows the substrate ion used. The third colum shows the starting position of the conserved arginine 173. This is either "in", pointing towards the heme iron, or "out" pointing towards the substrate entry channel. The fourth colum shows the oxidation state of the heme iron for the simulation. The last four colums show simulation details such as the amount of counter ions and water molecules, the box size, and the simulation length.

In this work, we study the binding of the low-spin ligand cyanide, a known inhibitor for heme oxidases, the substrate chlorite and the postulated intermediate hypochlorite to wild-type NdCld and the mutant R173A by means of molecular dynamics simulations in order to gain more information about the role of the flexible Arg173. Simulations were performed with the heme iron in its ferrous and ferric states, as well as compound I state (Table 1). Prior to the simulations, the series of ions ClO$^-$, ClO$_2^-$, ClO$_3^-$, and ClO$_4^-$ was parametrized for the GROMOS force field.[23,24] Our findings suggest that chlorite is attracted by the ferric state and that Arg173 plays a role in the initial substrate recognition, but not in the actual binding process, leading to the formation of the Fe(III)−ClO$_2$ complex. In contrast, the conserved basic amino acid seems to support the rebound mechanism by diminishing the escape of transiently formed hypochlorite. The findings are discussed with respect to experimental data on catalysis and inhibition of chlorite dismutase.

■ MATERIALS AND METHODS

Parametrization. Experimental absolute intrinsic hydration free energies, $\Delta_s G^\ominus$, for the series of Cl$^-$, ClO$^-$, ClO$_2^-$, ClO$_3^-$, and ClO$_4^-$ ions were derived based on available experimental data. This involved the formation enthalpy and entropy of the gas-phase ions, the conventional formation free energy of the aqueous ions, and an assumed absolute intrinsic proton hydration free energy of −1100 kJ·mol^{-1}.[25,26] The resulting absolute intrinsic hydration free energies are given in Table 2, and the

Table 2. Comparison between the Absolute Intrinsic Hydration Free Energy ($\Delta_s G^\ominus$) from Experimental Data and from Simulation[a]

ion	exptl $\Delta_s G^\ominus$ [kJ·mol^{-1}]	simul $\Delta_s G^\ominus$ [kJ·mol^{-1}]
Cl$^-$	−309.4	−310.2[b]
ClO$^-$	−335.0	−337.2
ClO$_2^-$	−310.6	−311.0
ClO$_3^-$	−240.7	−228.8
ClO$_4^-$	−227.1	−216.9

[a]A detailed derivation of the experimental values is outlined in the Supporting Information. [b]Value from Reif et al.[26]

detailed derivation is outlined in the Supporting Information, Table S1. Ions ClO$^-$, ClO$_2^-$, ClO$_3^-$, and ClO$_4^-$ were reparametrized to reproduce the experimental data. The raw simulation data was corrected by ex post calculations according to

$$\Delta_s G^\ominus = \Delta G_{chg}^{raw} + \Delta G_{cav} + \Delta G_{cor} + \Delta G_{std}^\ominus \quad (1)$$

where ΔG_{chg}^{raw} is the raw free energy of reversibly growing the partial charges of the atoms, ΔG_{cav} is the free energy of reversibly growing the van der Waals envelope of the neutral ion, and $\Delta G_{std}^\ominus = 7.95$ kJ·mol^{-1} is the standard-state correction[25,26] from equal concentrations in the gas and aqueous phase (simulated situation) to concentrations corresponding to a pressure of 1 bar in the gas phase and 1 m in the aqueous phase. ΔG_{cor} was calculated according to the correction scheme for oligo-atomic ion hydration[24] for the case of lattice-sum electrostatic interactions, as outlined in the Supporting Information.

Molecular Dynamics Simulations. Molecular dynamics simulations of the pentameric protein were performed using the GROMOS11 molecular simulation package.[27] Parameters from the GROMOS force field 54A7 were used. The parameters for the oxidized and reduced heme group were taken from Zou et al.[28] For compound I, an oxygen atom with GROMOS integer atom code 2 and a partial charge of −0.38e was covalently bound to the Fe ion with a bond length of 0.161 nm and O−Fe−N angles kept at 90° with a force constant of 380 kJ·mol^{-1}. The Fe ion maintained a partial charge of 0.48e, with the remaining charge distribution spread over the atoms of the porphyrin system by analogy to charge distributions from density functional calculations, kindly provided to us by Lars Olsen of the University of Copenhagen. Building blocks for all heme species are available in the Supporting Information.

The protein was solvated in simple point charge (SPC) water molecules[29] in a periodic rectangular simulation box to which chloride and sodium ions were added to obtain an overall neutral system at pH 7. The temperature of the systems was slowly increased to 300 K by 60 K every 20 ps and further equilibrated for 100 ps. A step size of 2 fs was used, and the coordinates were written out every 0.5 ps. A weak coupling with a relaxation time of 0.1 ps for the temperature and 0.5 ps for the pressure

was used to keep the temperature and pressure constant at 300 K and 1 atm, respectively.[30] The isothermal compressibility[31] was set to 4.575×10^{-4} (kJ·mol^{-1}·nm^{-3})$^{-1}$. The SHAKE algorithm[32] was used to constrain the bond lengths to their optimal values with a relative geometric accuracy of 10^{-4}. A molecular pairlist was generated using a triple-range cutoff.[33] Nonbonded interactions up to a short range of 0.8 nm were calculated at every time step from a pairlist that was updated every five steps. Interactions up to a long-range cutoff of 1.4 nm were calculated at pairlist updates and kept constant in between. A reaction-field contribution[34] was added to the electrostatic interactions and forces to account for a homogeneous medium with a dielectric permittivity of 61[35] outside the cutoff. A roto-translational constraint was used to prevent the protein from rotating in the rectangular box.[36] A summary of all performed simulations is given in Table 1.

Analysis. The GROMOS++ software package[37] was used to analyze the simulations. The atom-positional root-mean-square deviations of the backbone atoms from the initial model structures and the secondary structure according to the DSSP rules defined by Kabsch and Sander[38] were calculated to assess the stability of the protein. Hydrogen bonds were monitored based on the criterion that a hydrogen atom connected to a donor atom has an acceptor atom within 0.25 nm and the donor−hydrogen−acceptor angle is at least 135°.

■ RESULTS

Parametrization. The derivation of experimental reference values for the free energy of hydration is summarized in Table S1 (Supporting Information). Table 2 compares these data to the results from the simulations. The simulation data is calculated as the sum of a free energy of cavitation, a raw charging free energy, various corrections to account for artifacts in the treatment of electrostatic interactions, and a standard state correction (see Table S2, Supporting Information). When the absolute intrinsic hydration free energy ($\Delta_s G^{\ominus}$) of the parametrization is compared with those calculated from the experimental values (Table 2), the achieved absolute intrinsic hydration free energy ($\Delta_s G^{\ominus}$) from the parametrization is within an acceptable range of the experimental value and should render the ions compatible with the 54A7 and 54A8 GROMOS parameter sets.[23,24] The final interaction parameters are available from Table 3. Note that in the 54A8 parameter set, the charged groups of the protein have been parametrized accordingly, while this is not the case for the 54A7 parameter set.

Overall Protein Structure. After parametrization of the ions, a total of 12 simulations were performed with the pentameric chlorite dismutase from *Candidatus Nitrospira defluvii* (NdCld, PDB id 3nn1)[5] and its R173A mutant (PDB id 3nn3)[5] (Table 1). In order to assess the stability of the protein during the simulations and investigate possible structural changes, several analyses were performed on the last 10 ns of the simulations. The average values of various properties over the simulation and over the five monomers are presented in Table 4.

The atom-positional root-mean-square deviation (rmsd) with respect to the crystal structures 3nn1 and 3nn3 was in the range between 0.16 and 0.19 nm with a statistical uncertainty of 0.01−0.03 nm. No significant deviations from the crystal structure were observed. Moreover, the rmsd of the mutant is comparable to wild-type NdCld. Secondary structure elements over time were analyzed using the DSSP algorithm. The predominant α-helical structure (Figure 1) did not change significantly during the simulations. The percentage of amino

Table 3. Nonbonded and Bonded Parameters for the Ion Series

		Nonbonded Parameters		
ion	atom	IAC[a]	q [e]
Cl$^-$	Cl$^-$	38	−1
ClO$^-$	Cl	33	−0.17
	O	2	−0.83
ClO$_2^-$	Cl	33	0.55
	O	2	−0.775
ClO$_3^-$	Cl	33	−0.1
	O	2	−0.3
ClO$_4^-$	Cl	33	−0.2
	O	2	−0.2

		Bonded Parameters	
ion	property	minimum energy value	force constant
ClO$^-$	Cl−O bond	0.1758 nm	8.12×10^6 kJ·mol^{-1}·nm^{-4}
ClO$_2^-$	Cl−O bond	0.161 nm	4.84×10^6 kJ·mol^{-1}·nm^{-4}
	O−Cl−O angle	120.0°	780 kJ·mol^{-1}
ClO$_3^-$	Cl−O bond	0.153 nm	7.15×10^6 kJ·mol^{-1}·nm^{-4}
	O−Cl−O angle	108.0°	465 kJ·mol^{-1}
	improper dihedral	35.26439°	0.102 kJ·mol^{-1}·deg^{-2}
ClO$_4^-$	Cl−O bond	0.150 nm	8.37×10^6 kJ·mol^{-1}·nm^{-4}
	O−Cl−O angle	109.5°	450 kJ·mol^{-1}

[a]IAC refers to the integer atom code according to the GROMOS 54A7 force field.[23]

acids that are part of a helix over 10 ns of simulations over all five monomers ranges from 42.0% to 43.5% with a statistical uncertainty of 0.5% to 1.5% determined via block averaging.[39] In the crystal structures of wild-type NdCld and the variant R173A 43.9% and 44.3% of the amino acids are part of α-helical structures. The major helices did not unfold during the various simulations. Furthermore, the β-sheet structures at the center of each monomer were analyzed. The percentage of amino acids that are part of a β-sheet structure over the simulation time over all five monomers was found to range from 22.4% to 23.8% with a statistical uncertainty of 0.5% to 2.8%. This compares with 25.5% and 24.7% found in the crystal structures of the wild-type and mutant proteins. The absence of significant changes of secondary structure elements, as well as the low rmsd values for all simulations clearly suggest that the monomers of NdCld are very stable during the simulations.

Next we assessed the stability of the quaternary structure of NdCld by monitoring the number of hydrogen bonds between the monomers over time. The average number of hydrogen bonds over the last 10 ns of simulation over five interfaces ranges from 9.4 to 12.2 with a statistical uncertainty of 0.7 to 3.0 hydrogen bonds. This indicates that the monomers interact stably and the pentamer does not lose its quaternary structure over the course of the simulations.

Cyanide and Chlorite Binding to Ferrous and Ferric NdCld. The stability assessments described above clearly suggest that the overall structure of NdCld does not change during the 12 20-ns simulations. This concurs with the literature that heme enzymes do not undergo big structural changes during redox catalysis in general[11−13] thus allowing us to study the impact of the oxidation state of NdCld and the presence of various anions on the behavior of the fully conserved Arg173. The latter was shown to participate in the chlorite degradation mechanism[5,8,9] and to adopt two distinct conformations, one

Table 4. Overview of the Structural Parameters of the Simulations[a]

| simulation	RMSD [nm]	secondary structure [%]		number of hydrogen bonds
		helix	sheet	
OC	0.16 ± 0.01	42.8 ± 1.0	22.7 ± 0.5	11.0 ± 1.7
ON	0.16 ± 0.01	43.0 ± 0.5	23.5 ± 0.9	10.5 ± 0.7
OX	0.17 ± 0.01	42.4 ± 1.1	23.1 ± 0.9	10.4 ± 1.6
RC	0.16 ± 0.01	43.0 ± 1.1	22.9 ± 1.2	10.3 ± 2.5
RN	0.16 ± 0.01	42.9 ± 0.8	22.4 ± 1.5	11.4 ± 1.4
RX	0.18 ± 0.01	43.1 ± 1.0	23.8 ± 1.0	11.0 ± 1.4
CC	0.17 ± 0.01	42.9 ± 1.2	22.2 ± 2.8	11.6 ± 1.5
CI	0.16 ± 0.01	42.0 ± 1.5	22.6 ± 0.7	11.5 ± 3.0
MO	0.19 ± 0.02	42.6 ± 0.8	23.6 ± 1.3	10.9 ± 2.1
MC	0.19 ± 0.01	43.5 ± 1.5	22.8 ± 1.6	9.4 ± 1.9
OF	0.17 ± 0.02	42.7 ± 0.6	22.6 ± 0.8	10.7 ± 0.9
RF	0.18 ± 0.03	42.4 ± 1.1	23.1 ± 1.0	12.2 ± 0.8

[a]The first column shows the label of the simulation. The second column shows the root mean square deviation (RMSD) with respect to the crystal structure. The third column shows the amount of helices and sheets over the course of the simulations. The values for the crystal structures are 43.9% helices and 25.5% sheets for the wild-type structure and 44.3% helices and 24.7% sheets for the R173A mutant structure. The fourth column shows the amount of hydrogen bonds between the monomers. All values are averages over the last 10 ns of the simulation and over the five monomers with statistical uncertainties obtained from block averaging.[39]

pointing toward the heme iron (here referred to as "in") and one pointing toward the entry of the active site substrate access channel (here referred to as "out"). This prompted us to study the change in distance between the $C\zeta$ atom of Arg173 and the heme iron over the course of the simulations in all five monomers (Figure 2 and Table 5).

In the resting ferric state, R173 stayed in the "out" conformation as long as anions were absent in the initial protein structure (Figure 2G, simulation OX) or anions (e.g., chlorite) were free in solution (Figure 2I, simulation OF). In contrast, in ferrous NdCld R173 can adopt both positions (Figure 2H, simulation RX) with 38% in the "in" position and 62% in the "out" position (Table 5). Because the simulation was started with the arginine in the "out" position, transitions between the two conformations occurred during the 20 ns simulation. This indicates that the ferrous heme attracts the positively charged arginine at a distance within the cutoff chosen for the simulations (1.4 nm), in line with the average electrostatic potential calculated at the heme iron (Table 5). In the presence of chlorite in the solution (Figure 2J, simulation RF), R173 mainly adopted the "out" position (i.e., 4% "in" and 96% "out") most probably due to chlorite ions that came close to the active site.

With ferric NdCld and a cyanide ion (i.e., a low-spin ligand in heme proteins) in the active site and starting with R173 in the "out" position (simulation ON), during 85% of the simulation time, the arginine was in the "in" position. Apparently, the negatively charged cyanide ion represents a strong attractive force, which is also shown by on average 1.1 hydrogen bonds formed between the cyanide ion and R173. With ferrous NdCld and CN⁻ in the heme cavity (simulation RN), the "in"
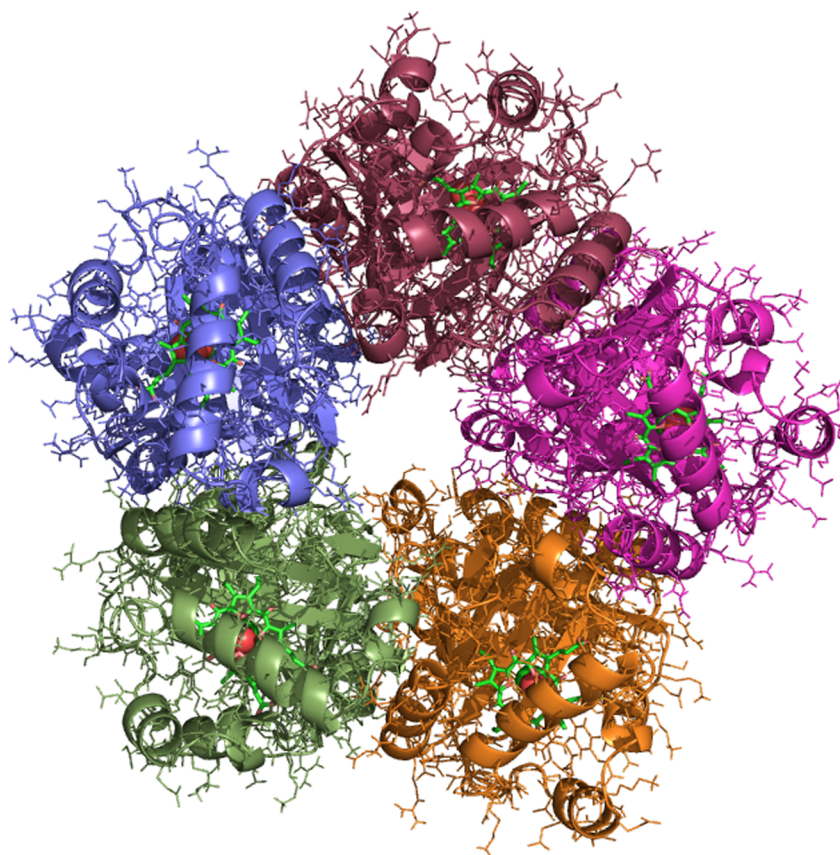
Figure 1. Structure of the pentameric chlorite dismutase from *Candidatus Nitrospira defluvii*. The five different monomers are colored differently, and the secondary structure elements are shown in a cartoon representation, while the side chains are shown as sticks. The heme is also shown with a stick representation, and the substrate ions in the active sites are shown with a bubble representation.
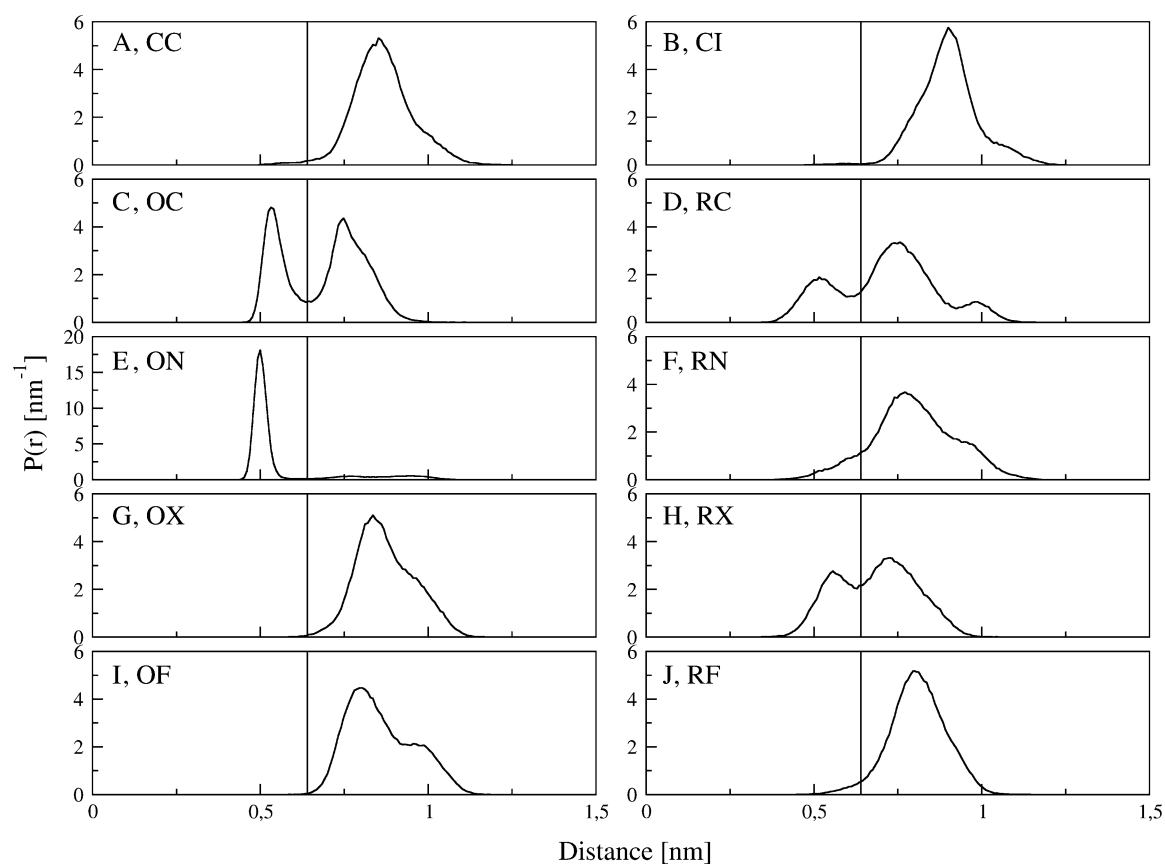
Figure 2. Normalized distributions of the distance between the heme iron and the Cζ atom of R173. The position of R173 is either "in", pointing toward the heme iron, or "out" pointing toward the substrate channel entry. The arginine was considered as "in" when then heme iron arginine distance was 0.64 nm or less. This threshold is represented by a vertical black bar in all graphs. Tile A shows the simulation with compound I, hypochlorite, and the arginine starting from an "out" position (CC). Tile B shows the simulation with compound I, hypochlorite, and the arginine starting from an "in" position (CI). Tiles C, E, and G show the simulations with ferric NdCld heme and chlorite, cyanide, and no ion, respectively (OC, ON, OX). Tiles D, F, and H show the simulations with ferrous NdCld heme and chlorite, cyanide, and no ion, respectively (RC, RN, RX). Tiles I and J show the simulations with 20 chlorite ions free in solution with the ferric and ferrous NdCld, respectively (OF, RF).

Table 5. Arginine 173 and Substrate Ion Positions[a]

simulation	arginine 173 [%]		substrate ion [%]		electrostatic potentional at the heme [kJ·mol^{-1}·e^{-1}]
	in	out	in	out	
OC	39	61	100	0	−202
ON	85	15	100	0	−279
OX	0	100			−152
RC	30	70	16	84	142
RN	11	89	4	96	136
RX	38	62			161
CC	1	99	7	93	−5
CI	1	99	8	92	29
MO			100	0	−231
MC			2	98	6
OF	0	100	3	97	−158
RF	4	96	0	100	141

[a]The first column shows the label of the simulation. The second column shows the percentage of the simulation time arginine 173 was in either the "in" position, pointing towards the heme iron or the "out" position pointing towards the substrate channel entry. The arginine was considered as "in" when then heme iron to arginine Cζ distance was 0.64 nm (corresponding to a minimum in distributions of Figure 2) or less. The third colum shows the percentage of the simulation time that the substrate ion was inside or outside one of the active sites of the pentamer. The ion was considered in the active site with a heme iron to ion distance of 0.8 nm (corresponding to the initial distances in simulations CC and CI, where the ions are furthest from the heme iron) or less. The fourth column shows the average electrostatic potential at the heme iron.

conformation was adopted only during 11% of the simulation time, most probably because the anion left the active site after a short period of time.

Next we placed the substrate chlorite in the heme cavity of either ferric or ferrous NdCld (Figure 2C,D, simulations OC and RC). In both cases, the amount of time that Arg173 spent
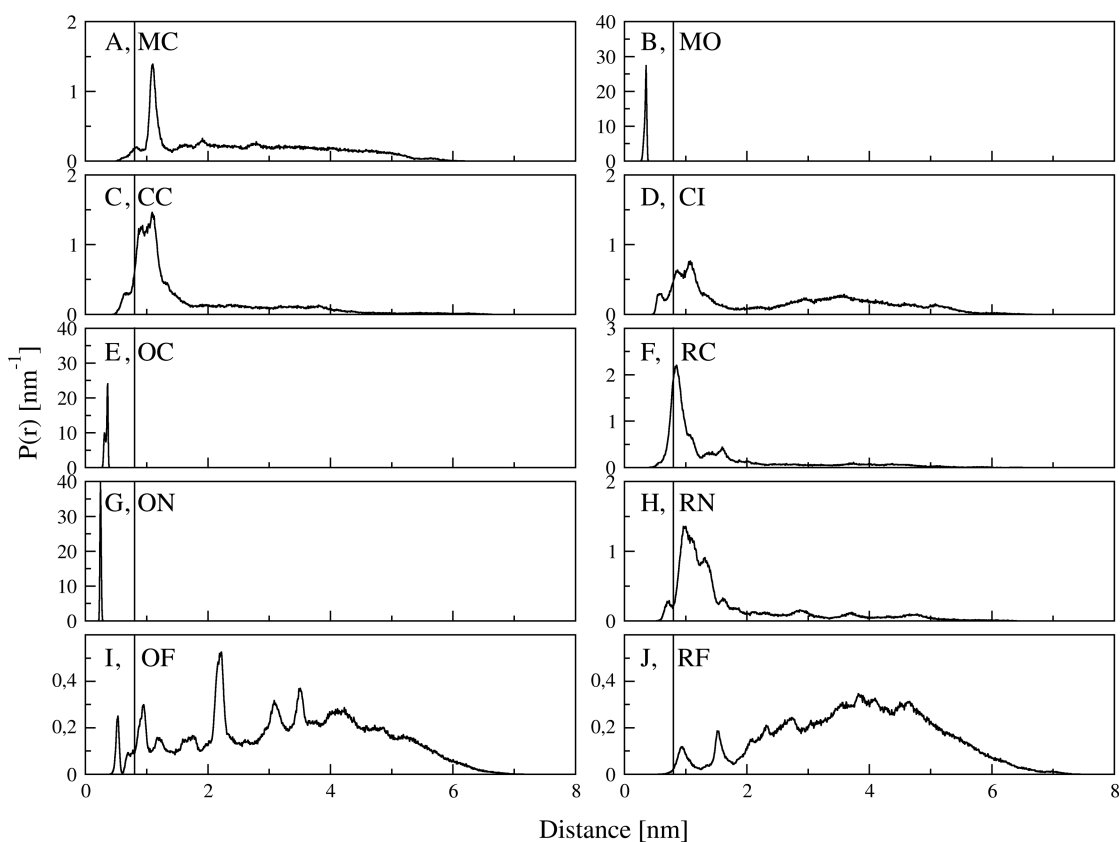
Figure 3. Normalized distributions of the position of the substrate ion. The substrate ion was considered inside the active site when the distance between the substrate ion and the heme iron was 0.8 nm or less. This threshold is shown by a vertical black bar in all graphs. Tiles A and B show the simulations with the R173A mutant structure and compound I and hypochlorite (MC) and ferric state and chlorite (MO), respectively. Tiles C and D show the simulations with compound I and hypochlorite with the conserved arginine 173 pointing toward the substrate channel entry (CC) or toward the heme iron (CI), respectively. Tiles E and G show the simulations with Fe(III) state and chlorite (OC) and cyanide (ON), respectively. Tiles F and H show the simulations with Fe(II) state and chlorite (RC) and cyanide (RN), respectively. Tiles I and J show the simulations with chlorite ions free in solution and ferric (OF) and ferrous (RF) NdCld, respectively.

in each position was similar (39% and 30% "in" versus 61% and 70% "out", respectively). However, the distance distribution with ferric NdCld showed two distinct peaks, whereas in the reduced protein three smaller and wider peaks were found, which might reflect substrate leaving the active site. The fact that with cyanide the arginine conformation is more balanced toward the "in" position could be due to the higher density of negative charges, while in the chlorite ion these are more delocalized over the atoms (Table 3). The higher attraction toward R173 of the cyanide versus the chlorite is also shown by only 0.6 hydrogen bonds between R173 and the chlorite, as opposed to 1.1 hydrogen bonds with cyanide. Note that as there are only a low number (between 4 and 5 over 20 ns) of reversible transitions observed, the percentages of the arginine positions are indications only.

Figure 3 depicts the distribution of the distance between the heme iron and the anions, whereas Table 5 summarizes the respective fraction being either in the heme cavity or outside. With ferric NdCld, both cyanide and chlorite remained close to the heme iron for 100% of the simulation time (Figure 3E,G, simulations OC and ON). In comparison, in the ferrous state, cyanide spent only 11% and chlorite 30% of the time in the active site. Figure 3F,H (simulations RC and RN) show that some ions moved as far as into the bulk water.

In two simulations (OF and RF), 20 chlorite ions were added to the water box. As can be seen in Figure 3I, some ions moved

into the active site of the ferric protein. An ion is considered inside the active site if the heme iron to ion distance is lower than 0.8 nm, which corresponds to the initial distances in simulations CC and CI, where the ions are furthest from the heme iron. In contrast, this did not occur in ferrous NdCld (Figure 3J). With ferrous NdCld, several chlorite ions came close to an active site, as shown in Figure 4B for the five ions that come closest to the 0.8 cutoff. However, these never entered the active site. In contrast, in ferric pentameric NdCld, four of the five active sites had chlorite close to the heme cavity during a large part of the simulation time, as shown in Figure 4A by the various curves. Two active sites completely bound a chlorite ion, which stayed in the active site for the rest of the simulation, depicted by the red and black lines in Figure 4A, which are significantly below the 0.8 nm cutoff. During the simulations, the active site was solvated, and no sodium or chlorite counterions were seen to enter the active site. Figure 5 demonstrates that the position of bound chlorite in this simulation (OF) was similar to the position in simulation OC, in which the substrate was in the active site from the beginning. During the simulations, no evidence was found that arginine mediates the shuttling of the ion to the active site. In contrast, Arg173 follows an anion that occupies the active site and adopts the "in" position only some time after the ion is already in the active site. In summary, spontaneous binding of the anionic substrate occurred during the 20 ns simulations of the ferric NdCld, and
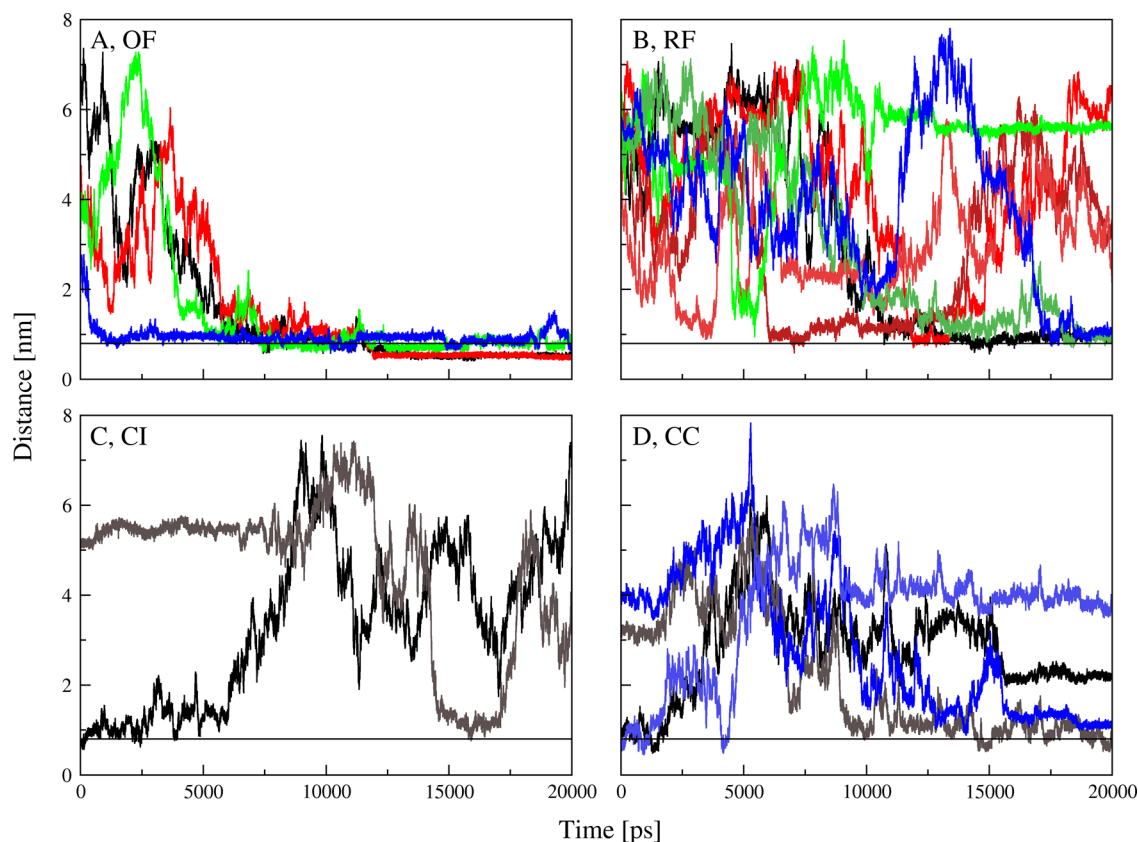
Figure 4. Distance between the substrate ions and the heme iron over the course of the simulations. The horizontal black line at 0.8 nm represents the threshold for considering an ion as being inside the active site or outside. Tile A shows the simulation with 20 chlorites free in solution and ferric NdclD (OF). Tile B shows the simulation with 20 chlorites free in solution and ferrous NdCld (RF). Tiles C and D show the simulations with compound I and hypochlorite and the conserved arginine 173 pointing toward the heme iron (CI) and toward the substrate channel entry (CC), respectively. For clarity, only curves for ions that show spontaneous binding are drawn in different colors. When two curves with matching colors are given, these are representative of a single ion interacting with multiple active sites.

anions bind tightly to the cavity, regardless of their character or the presence of Arg173. These findings clearly suggest that chlorite is attracted by the ferric heme state and that the role of Arg173 in the substrate binding process is negligible.

Hypochlorite Binding to Compound I. Hypochlorite has been postulated to be a transiently formed intermediate during the degradation of chlorite that reacts with compound I to form chloride and O_2. Simulating compound I and hypochlorite in the free solution showed that Arg173 adopts the "out" position almost exclusively (Figure 2A) regardless of its starting position.

Next we evaluated the distribution of the distance between the heme iron in the compound I state and hypochlorite with R173 either in the "in" or in the "out" conformation. In both simulations, most of the anions left the active site during the simulation (Figure 3C,D, simulations CC and CI, Table 5). Only 7% or 8% of the simulation time, ClO$^-$ was found in the heme cavity. This suggests that this transiently formed intermediate (in contrast to the substrate chlorite) easily escapes from the heme cavity and that the starting conformation of R173 does not matter for the hypochlorite retention.

Simulation of the mutant structure (R173A) with hypochlorite in the active site gave a similar picture. In contrast to the wild-type enzyme, ClO$^-$ spent only 2% of the simulation time in the heme cavity. The difference between wild-type and mutant protein is relatively small. However, it should be noted that in the wild-type enzyme the substrate ions stay significantly longer in the vicinity of the active site than in the mutant. By
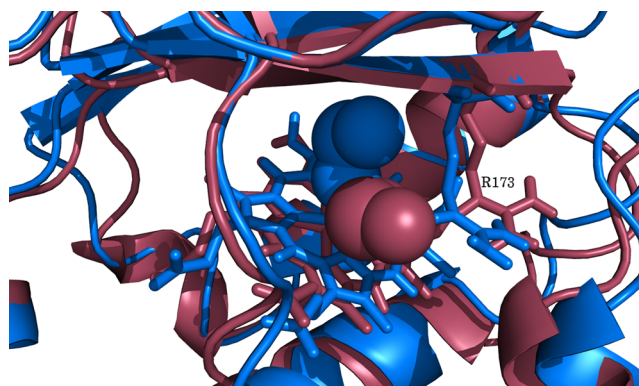
Figure 5. Overlay of one active site of the pentameric chlorite dismutase from *Candidatus Nitrospira defluvii* (NdCld) in the crystal structure with a chlorite bound (in blue) and after spontaneous binding during the simulation with 20 chlorite ions free in solution and an oxidized heme iron (in red). The R173 is pointing toward the substrate channel entry in both cases.

increasing the cutoff for being inside the active from 0.8 to 1.5, corresponding to the length of the substrate entry channel, we observed that hypochlorite ions stay 66% of the simulation time close to the active site, with only two ions leaving into the bulk water. In the mutant, the retention of ions was only observed for 29% of the time, with all ions in bulk water after 12 ns. It was previously suggested[17] that Arg173 helps to keep
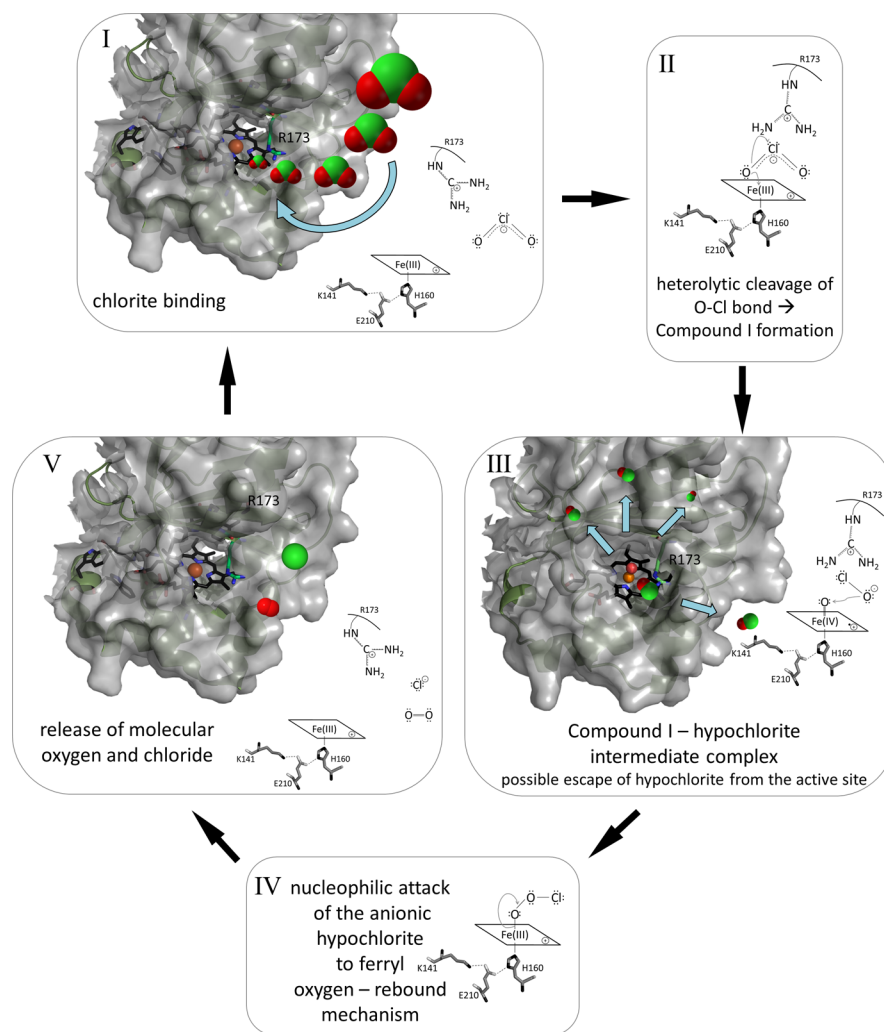
Figure 6. Proposed reaction cycle for chlorite dismutases. First (I) the substrate ClO_2^- binds to ferric NdCld forming the Fe(III)−ClO_2 adduct. R173 possibly plays a role in the initial recognition but is not crucial for the binding. This reaction is followed by oxidation (II) of the heme to compound I with concomitant reduction of chlorite to hypochlorite, ClO^-. Subsequently, (III) hypochlorite might escape the active site, which is hampered by R173, or (IV) the ferryl oxygen of compound I is rebound by hypochlorite, and (V) chloride and dioxygen are released.[16]

hypochlorite in the reaction sphere for the rebound mechanism. It has to be mentioned that in MD simulations using a classical force field description, no reaction can take place and a small difference in the residence time of hypochlorite may be sufficient to explain differences in the leaking behavior. Moreover, because a reaction could take place relatively quickly, it is impossible to quantitatively compare experimentally observed leaking rates to the ones observed in our simulations.

During the simulation of compound I with hypochlorite (CC and CI), most of the ions left the active site. But it was also observed that in some cases a hypochlorite ion returned to positions close to the active site, that is with a heme iron to ion distance lower than 0.8 nm, independent whether Arg173 was initially in the "in" or "out" position (Figure 4C,D). Analysis revealed that it was not the same hypochlorite that had left the active site previously. This can be seen following the black and gray curves in the Figure 4C,D. The lines represent the heme iron to ion distance of a hypochlorite ion during the simulation. The black line in tiles C and D of Figure 4 shows that the hypochlorite represented by that line is close to a heme iron at the beginning of the simulations but leaves during the

simulations. The distance between the same ion and another active site is represented by the gray line in tiles C and D of Figure 4, and it can be seen that the ion moves closely to the heme iron.

■ DISCUSSION

The pentameric chlorite dismutase from *Candidatus Nitrospira defluvii* in its ferrous, ferric, and compound I states was simulated in the presence of its substrate chlorite, the postulated intermediate hypochlorite, and the low-spin ligand cyanide in order to evaluate the role of the conserved distal arginine in these events. In functional Clds, Arg173 (NdCld numbering) represents the only charged amino acid in the heme cavity.

In Figure 6, we summarize the MD simulation data from this work and present a reaction mechanism that also incorporates the available experimental data. The initial reaction includes binding of the anionic substrate chlorite to the ferric resting state of NdClds forming the corresponding complex. Experimental data have shown that the role of Arg173 in this reaction is marginal. Exchange of R173 by either alanine or glutamine had only a small effect on the K_M value (i.e., increase by a factor of 1.3 in R173A compared with the wild-type protein).[9] This is

supported by the MD data, which showed that Arg173 does not play a role in shuttling the anion into the active site. It rather followed the charged molecules and changed its orientation ("in" versus "out") accordingly. Note that in the 54A7 force field, the intrinsic absolute free energy of hydration for the guanidinium ion is underestimated by ~15 kJ·mol^{-1},[24] potentially influencing the detailed equilibrium between the "in" and the "out" conformations. This might suggest that the role of Arg173 in this initial reaction step is substrate recognition, since no spontaneous binding events were observed in the simulation of the mutant Arg173Ala and hypochlorite leaking from the active site (simulation MC). In contrast, in both simulations with the wild-type NdCld and hypochlorite, some substrate ions returned to an active site after having left the protein (simulations CI and CC and Figure 4). This was also the case with both ferrous and ferric wild-type NdCld where some chlorite ions came close to the active site (simulations OF and RF, Figure 4). To confirm that R173 is relevant for substrate recognition, an additional simulation was run of the mutant in the ferric state with 20 chlorite ions randomly placed in the simulation box (cf. simulations OF and RF). No chlorite binding was observed in this simulation. Real binding was only observed with the ferric protein, which represents the resting state of chlorite dismutase, and with hypochlorite to the compound I state of the enzyme. The Fe(II) state does not participate in catalysis.

Binding of cyanide to the active site of heme proteins typically occurs with the respective ferric forms. The low-spin cyanide complexes of the corresponding Fe(II) forms are weak. Recent experimental data have demonstrated[9] that both the binding rate of cyanide to ferric NdCld and the stability of the low-spin complex was extremely low in NdCld mutants that lacked Arg173. The present MD study shows that cyanide remained in the heme cavity of wild-type ferric NdCld during simulation and promoted the "in" conformation of Arg173. With ferrous NdCld, cyanide easily escaped from the active site, and the "out" conformation of Arg173 prevailed.

Immediately after binding of the substrate chlorite to ferric NdCld, the heterolytic cleavage of chlorite occurs thereby oxidizing the enzyme to the compound I state and reducing chlorite to hypochlorite (Figure 6). This transient intermediate must stay in the reaction sphere for the subsequent recombination step. The turnover number (k_{cat}) for chlorite degradation in the mutant is ~6.5% (R173A)[9] compared with the wild-type enzyme. This underlines the importance of Arg173 in these reaction steps but also demonstrates that it is not fully essential for catalysis. Besides the decreased turnover number, the variant Arg173Ala was shown to be also more prone to inactivation than the wild-type enzyme.

The MD simulations of compound I with hypochlorite confirm that the conserved arginine 173 might play a role as already suggested[9,17] and that it is important to keep the transiently formed hypochlorite close to or in the active site. Recent experimental data suggest that some hypochlorite nevertheless escapes from the active site in a pH-dependent manner. As a consequence, the enzyme becomes irreversibly inactivated by oxidative modifications of both the protein matrix and the prosthetic group.[17] Escape of hypochlorite is more pronounced at high chlorite concentrations, as well as with mutant enzymes that lack Arg173. The present MD study clearly demonstrates that a large portion of hypochlorite escapes from the heme cavity and enters the bulk phase. This fits with the experimental data that reported oxidative modifications of amino acids on the surface of NdCld

that derive from hypochlorite.[17] The present findings also show that leakage of hypochlorite in the mutant R173A is higher than that in the wild-type protein although the MD simulations do not allow a correlation with experimental data since no recombination reaction can take place.

Chlorite dismutase is a promising biocatalyst that can be used for the degradation of anthropogenic chlorite contamination in the environment. For this purpose, it is necessary to select robust representatives or engineer the metalloenzymes and decrease their susceptibility for inactivation. The present study allowed new insights into the dynamics and the role of the conserved arginine in this process. It will be interesting to perform comparative studies of clade II dimeric chlorite dismutases, which are less prone to inactivation (unpublished data) but have a very similar heme cavity architecture.[7]

■ ASSOCIATED CONTENT

Ⓢ Supporting Information

Detailed derivation of experimental and calculated absolute intrinsic hydration free energies of the ions, molecular topology building blocks of the ions for the GROMOS force field, and molecular topology building blocks of the different heme species for the GROMOS force field. This material is available free of charge via the Internet at http://pubs.acs.org.

■ AUTHOR INFORMATION

Corresponding Author

*Chris Oostenbrink. Tel: (+43) 1/47654-8302. Fax: (+43) 1/47654-8309. E-mail: chris.oostenbrink@boku.ac.at.

Notes

The authors declare no competing financial interest.

■ ACKNOWLEDGMENTS

■ ABBREVIATIONS

Cld, chlorite dismutase; NdCld, pentameric chlorite dismutase from *Candidatus Nitrospira defluvii*; MD, molecular dynamics; OC, pentameric chlorite dismutase with a ferric heme and chlorite; ON, pentameric chlorite dismutase with a ferric heme and cyanide; OX, pentameric chlorite dismutase with a ferric heme and without a substrate ion; RC, pentameric chlorite dismutase with a ferrous heme and chlorite; RN, pentameric chlorite dismutase with a ferrous heme and cyanide; RX, pentameric chlorite dismutase with a ferrous heme and chlorite and without a substrate ion; CC, pentameric chlorite dismutase with compound I and hypochlorite, with the Arg173 facing out; CI, pentameric chlorite dismutase with compound I and hypochlorite, with the Arg173 facing in; MO, mutant pentameric chlorite dismutase (R173A) with a ferric heme and chlorite; MC, mutant pentameric chlorite dismutase (R173A) with compound I and hypochlorite; OF, pentameric chlorite dismutase with a ferric heme and chlorite free in solution; RF, pentameric chlorite dismutase with a ferrous heme and chlorite free in solution

■ REFERENCES

(1) Turano, P., and Lu, Y. (2001) Iron in heme and related proteins, *Handbook of metalloproteins*, pp 269–356, Marcel Dekker, Inc., New York.

(2) Ebihara, A., Okamoto, A., Kousumi, Y., Yamamoto, H., Masui, R., Ueyama, N., Yokoyama, S., and Kuramitsu, S. (2005) Structure-based functional identification of a novel heme-binding protein from Thermus thermophilus HB8. *J. Struct. Funct. Genomics* 6, 21–32.

(3) de Geus, D. C., Thomassen, E. A., Hagedoorn, P.-L., Pannu, N. S., van Duijn, E., and Abrahams, J. P. (2009) Crystal Structure of Chlorite Dismutase, a Detoxifying Enzyme Producing Molecular Oxygen. *J. Mol. Biol.* 387, 192–206.

(4) Goblirsch, B. R., Streit, B. R., DuBois, J. L., and Wilmot, C. M. (2010) Structural features promoting dioxygen production by Dechloromonas aromatica chlorite dismutase. *J. Biol. Inorg. Chem.* 15, 879–888.

(5) Kostan, J., Sjöblom, B., Maixner, F., Mlynek, G., Furtmüller, P. G., Obinger, C., Wagner, M., Daims, H., and Djinović-Carugo, K. (2010) Structural and functional characterisation of the chlorite dismutase from the nitrite-oxidizing bacterium "Candidatus Nitrospira defluvii": Identification of a catalytically important amino acid residue. *J. Struct. Biol.* 172, 331–342.

(6) Maixner, F., Wagner, M., Lücker, S., Pelletier, E., Schmitz-Esser, S., Hace, K., Spieck, E., Konrat, R., Le Paslier, D., and Daims, H. (2008) Environmental genomics reveals a functional chlorite dismutase in the nitrite-oxidizing bacterium 'Candidatus Nitrospira defluvii'. *Environ. Microbiol.* 10, 3043–3056.

(7) Mlynek, G., Sjöblom, B., Kostan, J., Füreder, S., Maixner, F., Gysel, K., Furtmüller, P. G., Obinger, C., Wagner, M., Daims, H., and Djinović-Carugo, K. (2011) Unexpected diversity of chlorite dismutases: A catalytically efficient dimeric enzyme from Nitrobacter winogradskyi. *J. Bacteriol.* 193, 2408–2417.

(8) Blanc, B., Mayfield, J. A., McDonald, C. A., Lukat-Rodgers, G. S., Rodgers, K. R., and DuBois, J. L. (2012) Understanding How the Distal Environment Directs Reactivity in Chlorite Dismutase: Spectroscopy and Reactivity of Arg183 Mutants. *Biochemistry* 51, 1895–1910.

(9) Hofbauer, S., Gysel, K., Bellei, M., Hagmüller, A., Schaffner, I., Mlynek, G., Kostan, J., Pirker, K. F., Daims, H., Furtmüller, P. G., Battistuzzi, G., Djinović-Carugo, K., and Obinger, C. (2014) Manipulating conserved heme cavity residues of chlorite dismutase: Effect on structure, redox chemistry, and reactivity. *Biochemistry* 53, 77–89.

(10) Hofbauer, S., Bellei, M., Sündermann, A., Pirker, K. F., Hagmüller, A., Mlynek, G., Kostan, J., Daims, H., Furtmüller, P. G., Djinović-Carugo, K., Oostenbrink, C., Battistuzzi, G., and Obinger, C. (2012) Redox Thermodynamics of High-Spin and Low-Spin Forms of Chlorite Dismutases with Diverse Subunit and Oligomeric Structures. *Biochemistry* 51, 9501–9512.

(11) Battistuzzi, G., Bellei, M., Bortolotti, C. A., and Sola, M. (2010) Redox properties of heme peroxidases. *Arch. Biochem. Biophys.* 500, 21–36.

(12) Bellei, M., Jakopitsch, C., Battistuzzi, G., Sola, M., and Obinger, C. (2006) Redox thermodynamics of the ferric-ferrous couple of wild-type synechocystis KatG and KatG(Y249F). *Biochemistry* 45, 4768–4774.

(13) Battistuzzi, G., Bellei, M., Zederbauer, M., Furtmüller, P. G., Sola, M., and Obinger, C. (2006) Redox thermodynamics of the Fe(III)/Fe(II) couple of human myeloperoxidase in its high-spin and low-spin forms. *Biochemistry* 45, 12750–12755.

(14) Battistuzzi, G., Bellei, M., De Rienzo, F., and Sola, M. (2006) Redox properties of the Fe3+/Fe2+ couple in Arthromyces ramosus class II peroxidase and its cyanide adduct. *J. Biol. Inorg. Chem.* 11, 586–592.

(15) Battistuzzi, G., Bellei, M., Borsari, M., Di Rocco, G., Ranieri, A., and Sola, M. (2005) Axial ligation and polypeptide matrix effects on the reduction potential of heme proteins probed on their cyanide adducts. *J. Biol. Inorg. Chem.* 10, 643–651.

(16) Lee, A. Q., Streit, B. R., Zdilla, M. J., Abu-Omar, M. M., and DuBois, J. L. (2008) Mechanism of and exquisite selectivity for O-O bond formation by the heme-dependent chlorite dismutase. *Proc. Natl. Acad. Sci. U. S. A.* 105, 15654–15659.

(17) Hofbauer, S., Gruber, C., Pirker, K. F., Schaffer, I., Jakopitsch, C., Sündermann, A., Oostenbrink, C., Furtmüller, P. G., and Obinger, C. (2014) Transiently produced hypochlorite is responsible for the irreversible inhibition of chlorite dismutase. *Biochemistry* 53, 3145–3157.

(18) Hagedoorn, P. L., de Geus, D. C., and Hagen, W. R. (2002) Spectroscopic characterization and ligand-binding properties of chlorite dismutase from the chlorate respiring bacterial strain GR-1. *Eur. J. Biochem.* 269, 4905–4911.

(19) Stenklo, K., Danielsson Thorell, H., Bergius, H., Aasa, R., and Nilsson, T. (2001) Chlorite dismutase from Ideonella dechloratans. *J. Biol. Inorg. Chem.* 6, 601–607.

(20) Mehboob, F., Wolterink, A. F. M., Vermeulen, A. J., Jiang, B., Hagedoorn, P.-L., Stams, A. J. M., and Kengen, S. W. M. (2009) Purification and characterization of a chlorite dismutase from Pseudomonas chloritidismutans. *FEMS Microbiol Lett.* 293, 115–121.

(21) Streit, B. R., and DuBois, J. L. (2008) Chemical and steady-state kinetic analyses of a heterologously expressed heme dependent chlorite dismutase. *Biochemistry* 47, 5271–5280.

(22) Streit, B. R., Blanc, B., Lukat-Rodgers, G. S., Rodgers, K. R., and DuBois, J. L. (2010) How active-site protonation state influences the reactivity and ligation of the heme in chlorite dismutase. *J. Am. Chem. Soc.* 132, 5711–5724.

(23) Schmid, N., Eichenberger, A. P., Choutko, A., Riniker, S., Winger, M., Mark, A. E., and van Gunsteren, W. F. (2011) Definition and testing of the GROMOS force-field versions 54A7 and 54B7. *Eur. Biophys. J.* 40, 843–856.

(24) Reif, M. M., Hünenberger, P. H., and Oostenbrink, C. (2012) New Interaction Parameters for Charged Amino Acid Side Chains in the GROMOS Force Field. *J. Chem. Theory Comput.* 8, 3705–3723.

(25) Hünenberger, P., and Reif, M. (2011) *Single-Ion Solvation*, RSC Theoretical and Computational Chemistry Series, Royal Society of Chemistry, Cambridge, U.K.

(26) Reif, M. M., and Hünenberger, P. H. (2011) Computation of methodology-independent single-ion solvation properties from molecular simulations. IV. Optimized Lennard-Jones interaction parameter sets for the alkali and halide ions in water. *J. Chem. Phys.* 134, No. 144104.

(27) Schmid, N., Christ, C. D., Christen, M., Eichenberger, A. P., and van Gunsteren, W. F. (2012) Architecture, implementation and parallelisation of the GROMOS software for biomolecular simulation. *Comput. Phys. Commun.* 183, 890–903.

(28) Zou, C., Larisika, M., Nagy, G., Srajer, J., Oostenbrink, C., Chen, X., Knoll, W., Liedberg, B., and Nowak, C. (2013) Two-dimensional heterospectral correlation analysis of the redox-induced conformational transition in cytochrome c using surface-enhanced Raman and infrared absorption spectroscopies on a two-layer gold surface. *J. Phys. Chem. B* 117, 9606–9614.

(29) Berendsen, H., Postma, J., Van Gunsteren, W., and Hermans, J. (1981) Interaction Models for Water in Relation to Protein Hydration, in *Intermolecular Forces* (Pullman, B., Ed.), pp 331–342, Reidel, Dordrecht, the Netherlands.

(30) Berendsen, H. J. C., Postma, J. P. M., van Gunsteren, W. F., DiNola, A., and Haak, J. R. (1984) Molecular dynamics with coupling to an external bath. *J. Chem. Phys.* 81, 3684–3690.

(31) van Gunsteren, W., Billeter, S., Eising, A., Hünenberger, P., Krüger, P., Mark, A., Scott, W., and Tironi, I. (1996) *Biomolecular Simulation: The GROMOS96 manual and userguide*, Hochschuleverlag AG, ETH, Zürich.

(32) Ryckaert, J.-P., Ciccotti, G., and Berendsen, H. J. (1977) Numerical integration of the cartesian equations of motion of a system with constraints: molecular dynamics of n-alkanes. *J. Comput. Phys.* 23, 327–341.

(33) Berendsen, H. J. C., van Gunsteren, W. F., Zwinderman, H. R. J., and Geurtsen, R. G. (1986) Simulations of Proteins in Water. *Ann. N.Y. Acad. Sci. 482*, 269−286.

(34) Tironi, I. G., Sperb, R., Smith, P. E., and van Gunsteren, W. F. (1995) A generalized reaction field method for molecular dynamics simulations. *J. Chem. Phys. 102*, 5451.

(35) Heinz, T. N., van Gunsteren, W. F., and Hünenberger, P. H. (2001) Comparison of four methods to compute the dielectric permittivity of liquids from molecular dynamics simulations. *J. Chem. Phys. 115*, 1125.

(36) Amadei, A., Chillemi, G., Ceruso, M. A., Grottesi, A., and Di Nola, A. (2000) Molecular dynamics simulations with constrained roto-translational motions: Theoretical basis and statistical mechanical consistency. *J. Chem. Phys. 112*, 9.

(37) Eichenberger, A. P., Allison, J. R., Dolenc, J., Geerke, D. P., Horta, B. A. C., Meier, K., Oostenbrink, C., Schmid, N., Steiner, D., Wang, D., and van Gunsteren, W. F. (2011) GROMOS++ Software for the Analysis of Biomolecular Simulation Trajectories. *J. Chem. Theory Comput. 7*, 3379−3390.

(38) Kabsch, W., and Sander, C. (1983) Dictionary of protein secondary structure: Pattern recognition of hydrogen-bonded and geometrical features. *Biopolymers 22*, 2577−2637.

(39) Allen, M., and Tildesley, D. (1989) *Computer Simulation of Liquids*, Oxford University Press, New York.